CARBON 78 (2014) 559–565

Available at www.sciencedirect.com

ScienceDirect

journal homepage: www.elsevier.com/locate/carbon

Strong ferromagnetism of reduced graphene oxide

Sai Qin [a], Xitao Guo [a], Yanqiang Cao [b], Zhenhua Ni [a], Qingyu Xu [a,c,d,*]

[a] Department of Physics & Key Laboratory of MEMS of the Ministry of Education, Southeast University, Nanjing 211189, China
[b] Department of Materials Science and Engineering, Nanjing University, Nanjing 210008, China
[c] National Laboratory of Solid State Microstructures, Nanjing University, Nanjing 210093, China
[d] Collaborative Innovation Center of Suzhou Nano Science and Technology, Soochow University, Suzhou 215123, China

ARTICLE INFO

Article history:
Received 25 December 2013
Accepted 12 July 2014
Available online 19 July 2014

ABSTRACT

The ferromagnetism of carbon-based materials has attracted much interest for its possible applications in spintronics devices. In this work, we studied the magnetic properties of reduced graphene oxide (rGO) obtained by high-temperature annealing of graphene oxide (GO) prepared in weak oxidizing conditions. The rGO samples exhibit strong room-temperature ferromagnetism, with saturation magnetization of 0.24 emu/g, about 24 times of the value of rGO prepared in strong oxidizing conditions. Hysteresis negative magnetoresistance (MR) has been observed in rGO, which confirms the intrinsic nature of the observed ferromagnetism. The MR value keeps nearly unchanged below 15 K, and decreases with further increasing temperature, and finally disappears at $T \geqslant 50$ K. At $T = 5$ K, the maximum MR ratio of $[R(H) - R(0)]/R(0)$ is about −2.5%. The strong ferromagnetism is attributed to the preserved graphitic structure of weakly oxidized rGO, and the negative MR is due to the spin dependent scattering of defects.

1. Introduction

Graphene, a single sheet of carbon atoms arranged in a honeycomb lattice, is one of the most fascinating materials in the last decade since its first report in 2004 [1]. Graphene possesses high carrier mobility, long spin lifetime, and limited hyperfine interaction, making it a very promising candidate for spintronics applications [2–4]. It has been predicted that ferromagnetism could exist in zigzag-edged graphene or semi-hydrogenated graphene sheets [5,6]. In the case of pristine graphene sheets, every carbon atom is sp^2 hybridized with three neighboring atoms and contributes to a delocalized π bonding network. Such configurations lead to its intrinsic diamagnetic properties [7]. Recent reports on the ferromagnetic (FM) properties of graphene suggest that the existence of various defects [8–10], half-hydrogenation corrugations [6,7,11,12], topological structures [13–15] in graphene can induce the carbon magnetism. Ning et al. have reported ferromagnetism in nanomesh graphene (NMG). The mesh structure with remarkable corrugations indicates the possible existence of the high density of defects in the NMG, which is believed to be the origin of ferromagnetism [16].

Aiming at molecular-based magnets, ferromagnetism in pure carbon-based materials is fundamentally and technologically important for many applications. Wang et al. have reported weak room temperature ferromagnetism of reduced graphene oxide (rGO) prepared in strong oxidizing environment [8]. Until recently, Khurana et al. have proven the temperature tuned defect induced magnetism in rGO [17]. Several theoretical studies have revealed that the main cause of ferromagnetism in graphene is due to various defects. The

* *Corresponding author at:* Department of Physics & Key Laboratory of MEMS of the Ministry of Education, Southeast University, Nanjing 211189, China.
E-mail address: xuqingyu@seu.edu.cn (Q. Xu).
http://dx.doi.org/10.1016/j.carbon.2014.07.039
0008-6223/

observed results suggested that these defects can be mended by treating the samples at elevated temperatures but sacrificing the ferromagnetism simultaneously [17]. This gives an inspiration that defects tuned by changing oxidizing condition may induce ferromagnetism in rGO. In present work, we found that rGO obtained by thermal reduction of graphene oxide (GO) prepared in weak oxidizing conditions has much stronger ferromagnetism than rGO prepared in strong oxidizing conditions. The observed hysteresis negative magnetoresistance (MR) confirms the intrinsic nature of the observed ferromagnetism.

2. Experimental details

GO was synthesized from natural graphite by a modified Hummer's method [18]. The graphite/$KMnO_4$ ratios of 2:3 and 2:6 were used to achieve weakly and strongly oxidized GO, respectively. The strongly and weakly oxidized GO are denoted as s-GO and w-GO, respectively. The rGO was synthesized from GO by annealing at 600 °C in Ar (flow rate as 30 sccm) for 1 h, which are denoted as s-rGO and w-rGO for strongly and weakly oxidized samples, respectively. The thicknesses of GO and rGO is 1–10 layers as determined by optical image and atomic force microscope, therefore it should be referred to few-layer GO and rGO.

The structures of GO and rGO were studied by Raman (Horiba Jobin Yvon LabRAM HR 800) and X-ray photoelectron spectroscopy (XPS, ThermoFisher SCIENTIFIC) with Al $K\alpha$ X- ray source ($h\nu$ = 1486.6 eV). The magnetic properties were measured by a physical property measurement system (PPMS-9, Quantum Design) from 10 to 300 K. MR was measured by a home-made magnetotransport measurement system with temperature down to 5 K and magnetic field up to 10 kOe. A Hall sensor was installed close to the sample to measure the magnetic field simultaneously during the MR measurements.

3. Results and discussion

Raman spectroscopy is an essential tool to characterize carbonaceous materials with ordered and disordered carbon structures [19]. Fig. 1 shows the typical Raman spectra of w-rGO and s-rGO. The Raman spectrum of w-rGO (Fig. 1a) shows a strong D peak at 1366 cm^{-1} due to the κ-point phonons of A_{1g} and a G peak at 1594 cm^{-1} corresponding to the first-order scattering of the E_{2g} mode symmetry [20]. The Raman spectrum of s-rGO (Fig. 1b) contains both D and G bands (at 1349 and 1591 cm^{-1}, respectively), but with a decreased D/G intensity ratio (1.1) compared to that in w-rGO (1.6). Higher D/G ratio in w-rGO suggests that it has better graphitic structure compared to s-rGO [21]. The origin of D band is attributed to the formation of defects and disorder such as the presence of in-plane hetero-atoms, grain boundaries, aliphatic chain, etc. [22], the strong D band in rGO samples suggest that they contain a great amount of defects, which is favorable for the occurrence of ferromagnetism, although not all kinds of defects will produce ferromagnetism.

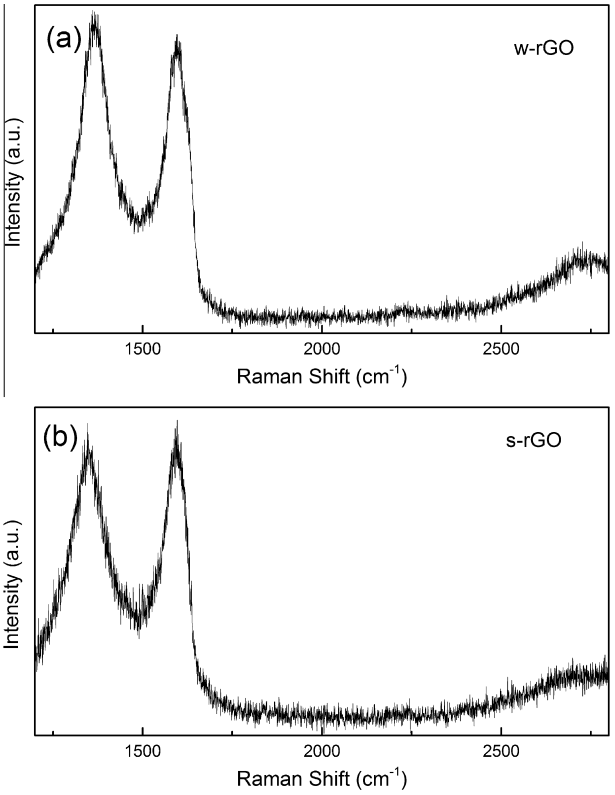

Fig. 1 – Raman spectra of (a) w-rGO and (b) s-rGO.

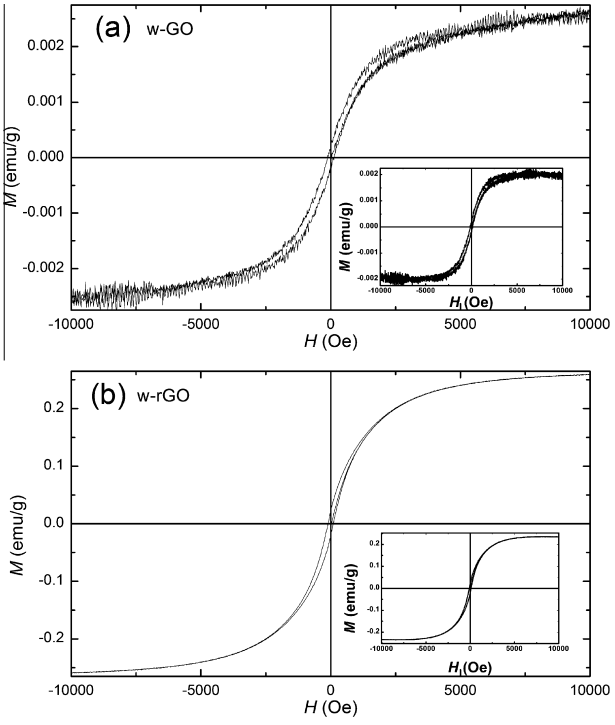

Fig. 2 – *M–H* curves for (a) w-GO and (b) w-rGO at 300 K. Insets show the FM magnetization of w-GO (top) and w-rGO (bottom) after subtracting the high field linear background.

Fig. 2 shows *M–H* curves of w-GO and w-rGO at 300 K in the field range of -10 kOe < *H*<+10 kOe. Very weak ferromagnet-

ism can be observed in w-GO, superimposed on the paramagnetism. After subtracting the high field linear background, the FM contribution can be obtained with saturation FM magnetization (M_s) of 0.002 emu/g, as shown in the inset. After reduction, strongly enhanced ferromagnetism has been observed in w-rGO, with M_s of 0.24 emu/g for w-rGO, which is 12 times of that of rGO reported by Wang et al. (0.02 emu/g at room temperature) [8] and 6 times of that of NMG reported by Ning et al. (0.04 emu/g) [16]. To check the possible contribution from magnetic impurities, the highly sensitive technique of inductively coupled plasma (ICP) analysis was performed, the total amount of magnetic impurities (Fe 250 ppm, Co 2 ppm, Ni 37 ppm) in w-rGO was determined to be below 300 ppm. An Fe impurity content of 1 μg g^{-1} would give the magnetization of 2.2×10^{-4} emu/g [23]. The observed FM magnetization for w-rGO (0.24 emu/g at 300 K) should correspond to 1090 ppm of Fe (or 8015 ppm Ni and 3000 ppm Co) [24]. These results exclude the extrinsic origin and confirm the intrinsic nature of the observed ferromagnetism, which might originate from the remaining graphitic structure and possible H absorption [25,26]. The expected M_s for graphene should be 502 emu/g [27], assuming all the carbon atoms have a FM unpaired electron. Thus, the observed M_s (0.24 emu/g) at 300 K for w-rGO corresponds to ~0.05% carbon atoms. Usually, defects such as vacancies, adatoms, and zigzag edges can produce localized magnetic moments by the formation of unpaired spins [8–10,28–31]. However, by the loss of graphene's structural stability, the vacancy-induced magnetic moment was limited [10]. Atoms (molecules) adsorbed at the same sublattice coupled ferromagnetically, while no magnetism or antiferromagnetism is found for adsorbates at opposite sublattices [32,33]. The edge states localized around the zigzag edge region have localized spins, which behave cooperatively with each other forming a magnetically ordered state, while they are completely absent from the armchair edge [31]. These cases make the obtained M_s much smaller than 502 emu/g. The coercivity (H_c) is 131 and 102 Oe, for w-GO and w-rGO respectively, which is slightly larger than that of rGO reported by Wang et al. [8]. Fig. 3a shows the *M–H* loops of w-GO at 10 K, which shows the enhanced paramagnetism with negligible ferromagnetism. The M_s of w-rGO is 0.26 emu/g, which is nearly the same as the value at 300 K. The increased slope at high field indicates the enhanced paramagnetic contribution at 10 K for w-rGO.

The results of temperature-dependent magnetization (*M–T*) measurements for w-GO and w-rGO are shown in Fig. 4a and b, which were measured in the presence of 2 kOe during the warming processes to 300 K after cooling down from 300 K under 2 kOe. For w-GO, the magnetization increases with decreasing temperature, and sharp rise can be observed below 30 K (Fig. 4a). This phenomenon is similar to that in oxidized unzipped and chemically converted graphene nanoribbons reported by Rao et al. [13]. The w-GO exhibits the typical paramagnetic behavior, with low-field susceptibility $\chi = M/H$ following the Curie law $\chi \propto 1/T$ (inset). For w-rGO (Fig. 4b), a drastic decrease of magnetization with increasing temperature below 30 K, followed by the gradual decrease with further increasing temperature. Quite large magnetization can still be observed at room temperature,

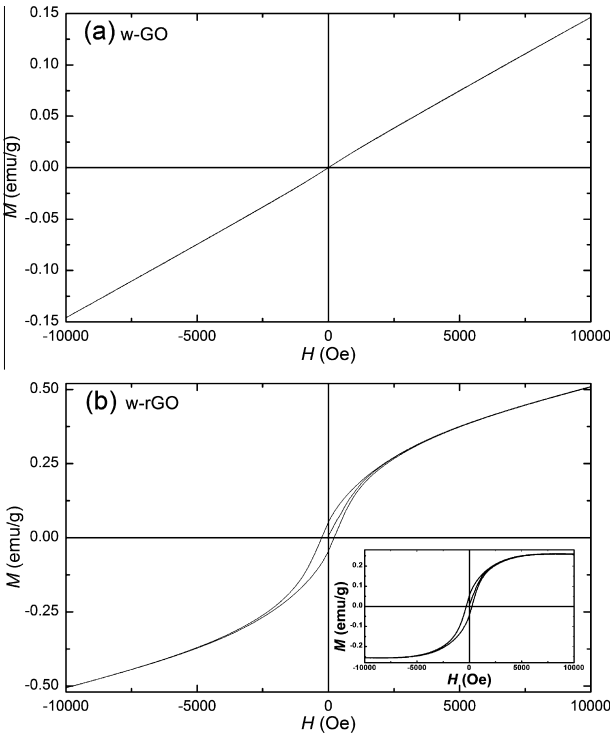

Fig. 3 – *M–H* curves for (a) w-GO and (b) w-rGO at 10 K. Inset shows the FM magnetization of w-rGO after subtracting the high field linear background.

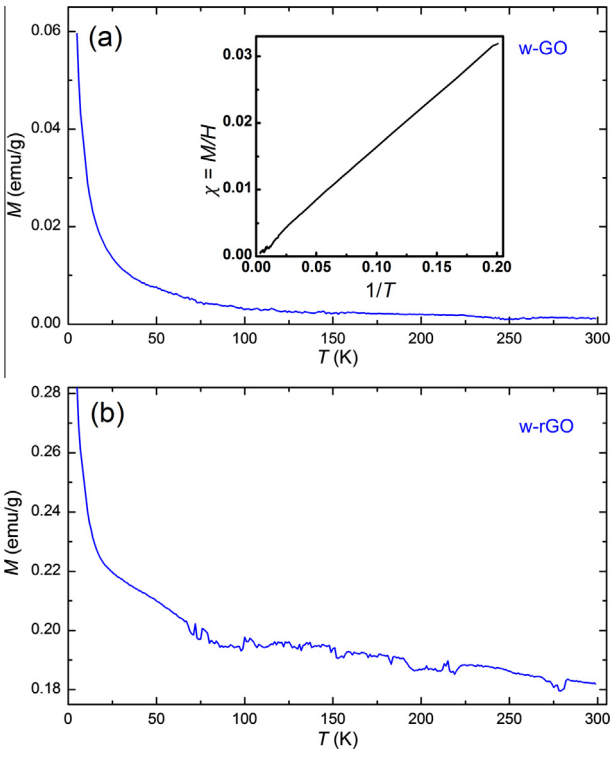

Fig. 4 – *M–T* curves for (a) w-GO and (b) w-rGO under 2 kOe. Inset is the $\chi - 1/T$ curve for GO. (A color version of this figure can be viewed online.)

confirming the FM properties. The *M–T* curve for w-rGO suggests the coexistence of paramagnetism and ferromagnetism.

Fig. 5 shows *M–H* curves for s-GO and s-rGO at 300 K, with FM magnetization shown in the insets. Feeble M_s of 0.0005 emu/g is found for s-GO, which is only one fourth of the value of w-GO (0.002 emu/g, Fig. 2a). FM hysteresis loop from s-rGO (Fig. 5b) is clearly seen, with M_s of 0.01 emu/g, which is much less than that of w-rGO (0.24 emu/g, Fig. 2b). The H_c is 110 and 121 Oe, for s-GO and s-rGO, respectively, which is close to that of w-GO (131 Oe) and w-rGO (102 Oe). At 10 K, strongly enhanced paramagnetism can be observed for both s-GO and s-rGO (Fig. 6). The linear *M–H* curve suggests the negligible ferromagnetism in s-GO. Weak ferromagnetism can be observed for s-rGO. The M_s is only 0.04 emu/g, significantly smaller compared with w-rGO (0.26 emu/g at 10 K).

A deeper analysis of the moieties present in rGO has been made with the aid of XPS. Fig. 7a and b shows the C1s XPS spectra of w-GO and w-rGO. The deconvolution of the C1s peak of w-GO displays three peaks locating at binding energies of 284.8, 286.8 and 288.2 eV, which can be assigned to the C—C (C=C), C—O and O=C—OH (carboxylate C) functional groups, respectively [34–36]. The C1s XPS spectrum of w-rGO also contains similar functional groups, as shown in Fig. 7b, but the intensity of oxygen-containing functional groups is much lower than that of w-GO. Upon thermal reduction, a new functional group π–π^* (291.9 eV) appears in w-rGO [37]. There are a variety of defects in carbon materials, such as vacancies, adatoms, the vacancy-hydrogen complexes and fragments with zigzag edges, which can produce magnetic moments. For rGO, due to the removal of oxygen-containing

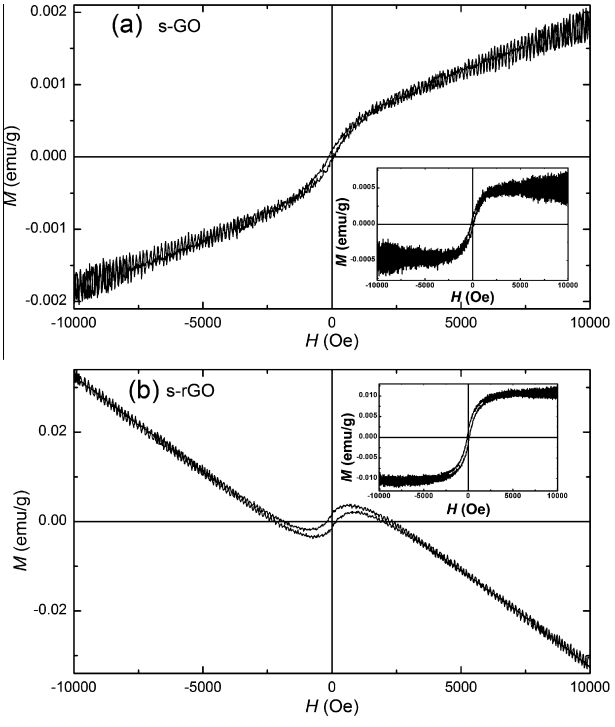

Fig. 5 – *M–H* curves for (a) s-GO and (b) s-rGO at 300 K. Insets show FM magnetization of s-GO (top) and s-rGO (bottom) after subtracting the high field linear background.

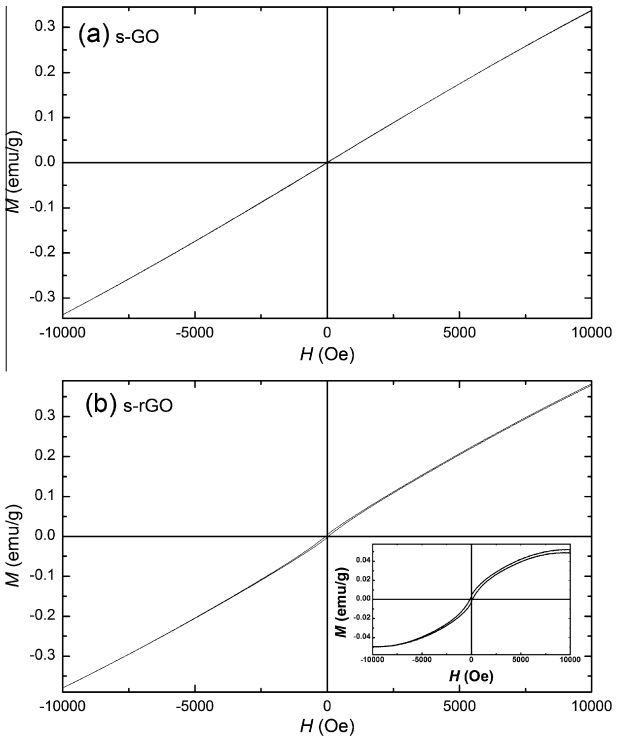

Fig. 6 – *M–H* curves for (a) s-GO and (b) s-rGO at 10 K. Inset shows FM magnetization of s-rGO after subtracting the high field linear background.

functional groups during annealing, vacancies and topological defects with unpaired electrons and net spins would be introduced on the graphene sheets [8], and these defect sites contain spins which participate in ferromagnetism [17]. The C1s spectra of s-GO and s-rGO are shown in Fig. 7c and d. Clearly, the C1s spectrum of s-GO exhibits similar kinds of oxygen-containing functional groups as w-GO, while their peak intensities are slightly larger. Reduction of potassium permanganate mass can effectively reduce the O=C—OH (carboxylate C) and C–O functional groups in rGO (compared with s-rGO) which result in better graphitic structure in w-rGO, leading to the enhancement of ferromagnetism [25].

In order to further check the intrinsic nature of the ferromagnetism in w-rGO and its possible spintronics applications, we measured MR of w-rGO by four-terminal method. The w-rGO powders were pressed into a 5 mm-diameter piece, which was from the same batch of w-rGO for the other characterizations. The MR results are shown in Fig. 8 in the field range of $-10\ \text{kOe} < H < 10\ \text{kOe}$. The MR value is defined as $[R(H) - R(0)]/R(0)$, where $R(0)$ is the resistance at zero field. Hysteresis negative MR curve can be observed at low temperatures. Fig. 9 shows the temperature dependence of MR, and the inset shows the temperature dependent resistance curve. The increasing resistance with decreasing temperature indicates the semiconductor behavior of w-rGO. The MR value is about −2.5% below 15 K, and decreases with increasing temperature above 15 K, and disappears at $T \geqslant 50$ K. Similar negative hysteresis MR with temperature dependence has been reported by Barzola-Quiquia et al., which is a clear indication of the intrinsic nature of the observed ferromagnetism

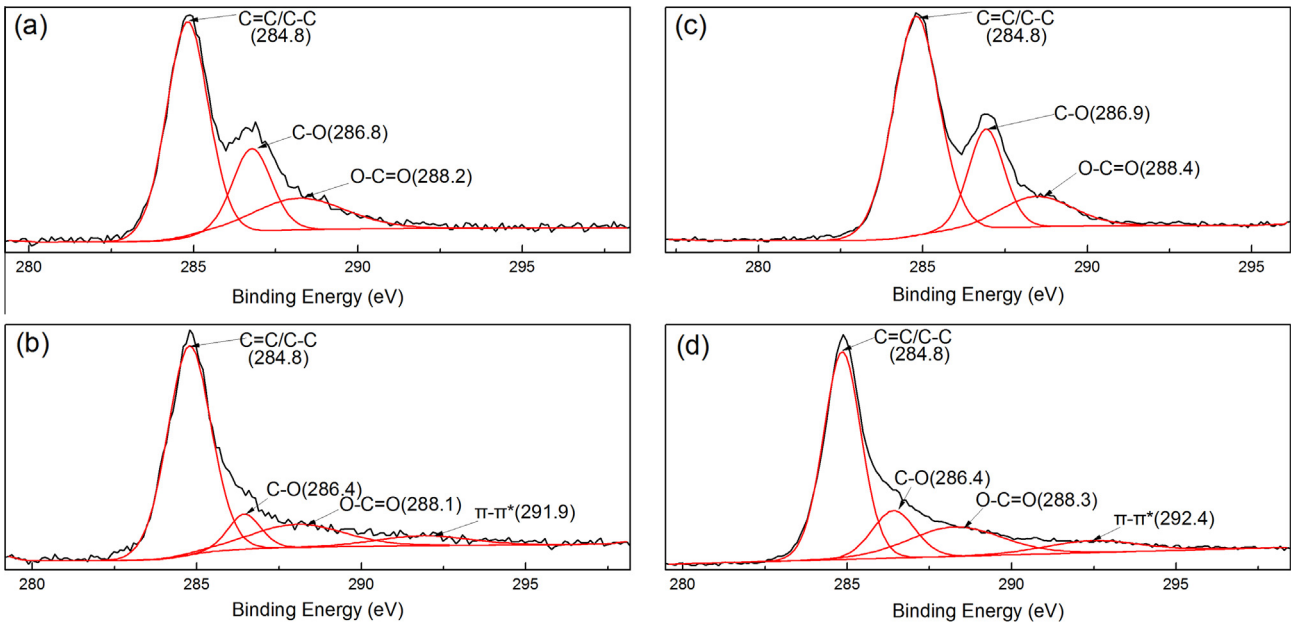

Fig. 7 – The C1s XPS spectra of (a) w-GO, (b) w-rGO, (c) s-GO and (d) s-rGO. (A color version of this figure can be viewed online.)

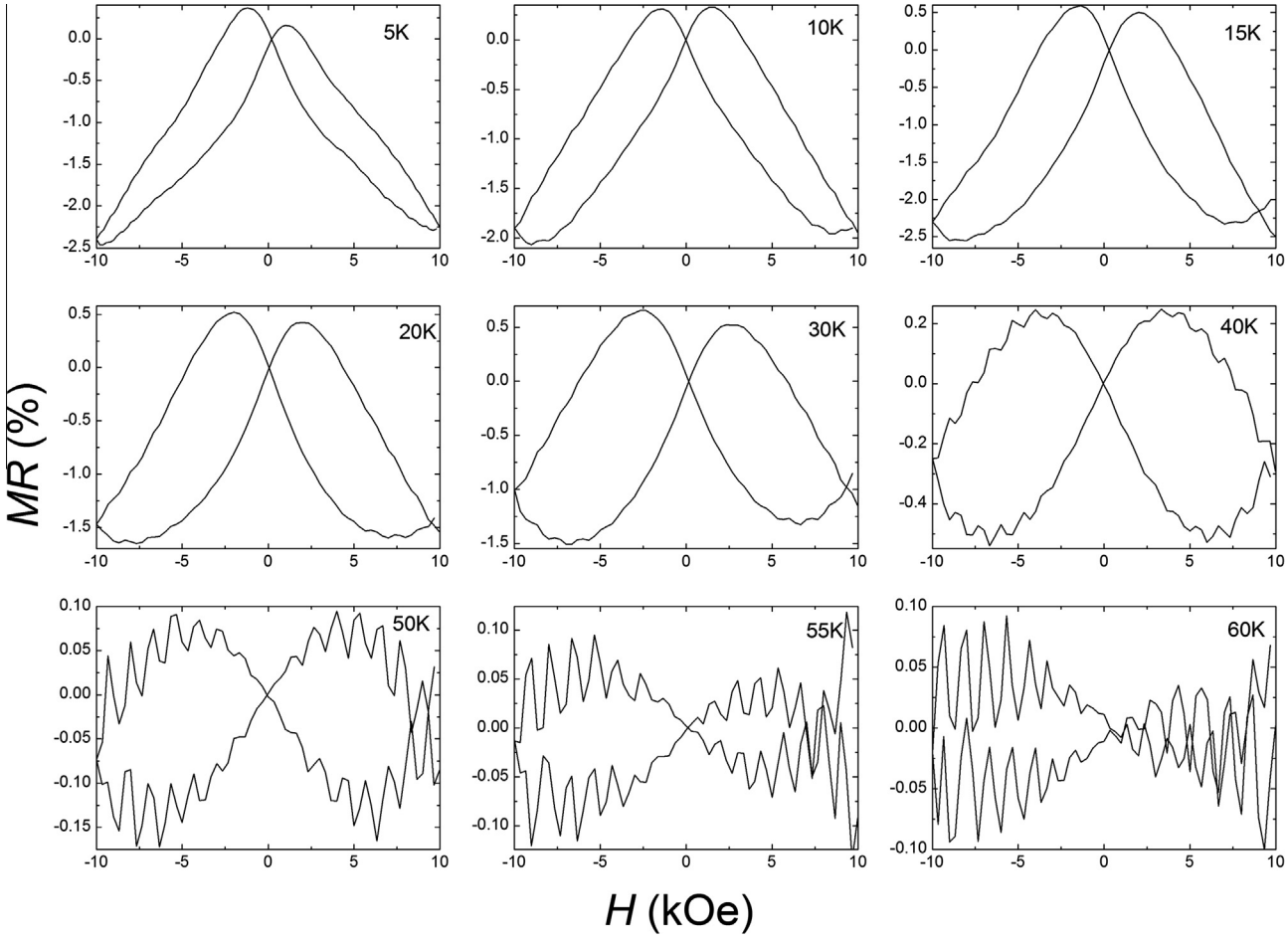

Fig. 8 – MR curves of w-rGO measured at different temperature.

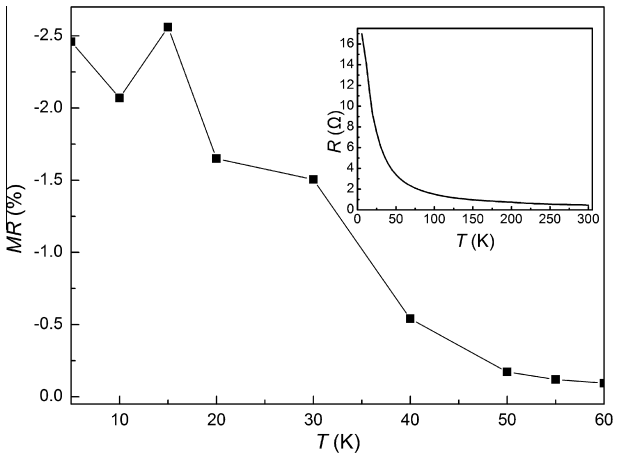

Fig. 9 – Temperature dependent MR of w-rGO. Inset is the temperature dependent resistance.

[38]. There are both positive [39] and negative [40,41] MR effects in graphene. The negative MR may be attributed to the reduction of quantum confinement through the formation of cyclotron orbits and the delocalization effect under the magnetic field [42–47]. The positive MR is caused by weak antilocalization due to the chiral nature of electrons in a monolayer of graphite (graphene) [48], or the inhomogeneous charge distribution due to charged impurities which creates a random resistor network [49]. Both positive and negative MR curves in nonmagnetic graphene have no hysteresis loop. The observed negative hysteresis loop of MR for our w-rGO sample can be attributed to the spin dependent scattering of the FM defects, and proves the intrinsic nature of the observed ferromagnetism. At 10 K, the peak position of MR curve for w-rGO is about 1500 Oe, which is much larger than H_c of 240 Oe. The MR peak positions further shift to higher field with increasing temperature. The detailed mechanism is still unclear. We suggest that it might be due to the superposition of the positive MR and negative MR in rGO, leading to the higher field of the MR peak position compared with the corresponding *M–H* curve. The strong decrease of the negative MR and the relatively temperature independent positive MR shift the MR peak positions to higher fields with increasing temperature.

4. Conclusions

In summary, strongly enhanced ferromagnetism has been observed in rGO prepared in the weak oxidizing conditions. The M_s of w-rGO (0.24 emu/g) is about 24 times of the value of s-rGO prepared in strong oxidizing environment (0.010 emu/g) measured at 300 K. We have observed hysteresis curves of negative MR in w-rGO at temperatures below 50 K due to the spin dependent scattering by the magnetic defects, confirming the intrinsic nature of the ferromagnetism.

Acknowledgements

This work is supported by National Key Projects for Basic Researches of China (2010CB923404), the National Natural Science Foundation of China (51172044, 61376104, and 11104026), the Natural Science Foundation of Jiangsu Province of China (BK2011617, and BK2011585), the 333 Project of Jiangsu Province, the Scientific Research Foundation for the Returned Overseas Chinese Scholars, State Education Ministry.

REFERENCES

[1] Novoselov KS, Geim AK, Morozov SV, Jiang D, Zhang Y, Dubonos SV, et al. Electric field effect in atomically thin carbon films. Science 2004;306(5696):666–9.
[2] Novoselov KS, Geim AK, Morozov SV, Jiang D, Katsnelson MI, Grigorieva IV, et al. Two-dimensional gas of massless Dirac fermions in graphene. Nature 2005;438:197–200.
[3] Kane CL, Mele EJ. Quantum spin Hall effect in graphene. Phys Rev Lett 2005;95:226801.
[4] Tombros N, Jozsa C, Popinciuc M, Jonkman HT, van Wees BJ. Electronic spin transport and spin precession in single graphene layers at room temperature. Nature 2007;448:571–4.
[5] Soriano D, Muñoz-Rojas F, Fernández-Rossier J, Palacios JJ. Hydrogenated graphene nanoribbons for spintronics. Phys Rev B 2010;81:165409.
[6] Zhou J, Wang Q, Sun Q, Chen XS, Kawazoe Y, Jena P. Ferromagnetism in semihydrogenated graphene sheet. Nano Lett 2009;9(11):3867–70.
[7] Xie L, Wang X, Lu J, Ni Z, Luo Z, Mao H, et al. Room temperature ferromagnetism in partially hydrogenated epitaxial graphene. Appl Phys Lett 2011;98:193113.
[8] Wang Y, Huang Y, Song Y, Zhang X, Ma Y, Liang J, et al. Room-temperature ferromagnetism of graphene. Nano Lett 2009;9(1):220–4.
[9] Rout CS, Kumar A, Kumar N, Sundaresan A, Fisher TS. Room-temperature ferromagnetism in graphitic petal arrays. Nanoscale 2011;3:900–3.
[10] Nair RR, Sepioni M, Tsai I-L, Lehtinen O, Keinonen J, Krasheninnikov AV, et al. Spin-half paramagnetism in graphene induced by point defects. Nat Phys 2012;8:199–202.
[11] Šljivančanin Ž, Balog R, Hornekær L. Magnetism in graphene induced by hydrogen adsorbates. Chem Phys Lett 2012;541:70–4.
[12] Tada K, Haruyama J, Yang HX, Chshiev M, Matsui T, Fukuyama H. Ferromagnetism in hydrogenated graphene nanopore arrays. Phys Rev Lett 2011;107:217203.
[13] Rao SS, Jammalamadaka SN, Stesmans A, Moshchalkov VV, van Tol J, Kosynkin DV, et al. Ferromagnetism in graphene nanoribbons: split versus oxidative unzipped ribbons. Nano Lett 2012;12(3):1210–7.
[14] Kan M, Zhou J, Sun Q, Wang Q, Kawazoe Y, Jena P. Tuning magnetic properties of graphene nanoribbons with topological line defects: from antiferromagnetic to ferromagnetic. Phys Rev B 2012;85:155450.
[15] Poumirol J-M, Cresti A, Roche S, Escoffier W, Goiran M, Wang X, et al. Edge magnetotransport fingerprints in disordered graphene nanoribbons. Phys Rev B 2010;82:041413.
[16] Ning G, Xu C, Hao L, Kazakova O, Fan Z, Wang H, et al. Ferromagnetism in nanomesh graphene. Carbon 2013;51:390–6.
[17] Khurana G, Kumar N, Kotnala RK, Nautiyal T, Katiyar RS. Temperature tuned defect induced magnetism in reduced graphene oxide. Nanoscale 2013;5:3346–51.
[18] Hummers WS, Offeman RE. Preparation of graphitic oxide. J Am Chem Soc 1958;80(6):1339.

[19] Rao CNR, Biswas K, Subrahmanyam KS, Govindaraj A. Graphene, the new nanocarbon. J Mater Chem 2009;19:2457–69.
[20] Tuinstra F, Koenig JL. Raman spectrum of graphite. J Chem Phys 1970;53(3):1126–30.
[21] Ferrari AC, Robertson J. Interpretation of Raman spectra of disordered and amorphous carbon. Phys Rev B 2000;61:14095–107.
[22] Krishnamoorthy K, Veerapandian M, Yun K, Kim SJ. The chemical and structural analysis of graphene oxide with different degrees of oxidation. Carbon 2013;53:38–49.
[23] Esquinazi P, Setzer A, Höhne R, Semmelhack C, Kopelevich Y, Spemann D, et al. Ferromagnetism in oriented graphite samples. Phys Rev B 2002;66:024429.
[24] Eng AYS, Poh HL, Sanek F, Marysko M, Matejkova S, Sofer Z, et al. Searching for magnetism in hydrogenated graphene: using highly hydrogenated graphene prepared via birch reduction of graphite oxides. ACS Nano 2013;7(7):5930–9.
[25] Ohldag H, Tyliszczak T, Höhne R, Spemann D, Esquinazi P, Ungureanu M, et al. π-Electron ferromagnetism in metal-free carbon probed by soft X-ray dichroism. Phys Rev Lett 2007;98:187204.
[26] Ohldag H, Esquinazi P, Arenholz E, Spemann D, Rothermel M, Setzer A, et al. The role of hydrogen in room-temperature ferromagnetism at graphite surfaces. New J Phys 2010;12(12):123012.
[27] Murata K, Ueda H, Kawaguchi K. Preparation of carbon powders by pyrolysis of cyclododecane under vacuum and their magnetic properties. Synth Met 1991;44:357–62.
[28] Feng Q, Tang N, Liu F, Cao Q, Zheng W, Ren W, et al. Obtaining high localized spin magnetic moments by fluorination of reduced graphene oxide. ACS Nano 2013;7(8):6729–34.
[29] Kobayashi K. Electronic structure of a stepped graphite surface. Phys Rev B 1993;48:1757.
[30] Klein DJ. Graphitic polymer strips with edge states. Chem Phys Lett 1994;217(3):261–5.
[31] Enoki T, Kobayashi Y, Fukui KI. Electronic structures of graphene edges and nanographene. Int Rev Phys Chem 2007;26(4):609–45.
[32] Boukhvalov DW, Katsnelson MI, Lichtenstein AI. Hydrogen on graphene: electronic structure, total energy, structural distortions and magnetism from first-principles calculations. Phys Rev B 2008;77:035427.
[33] Yazyev OV, Helm L. Defect-induced magnetism in graphene. Phys Rev B 2007;75:125408.
[34] Stankovich S, Dikin DA, Piner RD, Kohlhaas KA, Kleinhammes A, Jia Y, et al. Synthesis of graphene-based nanosheets via chemical reduction of exfoliated graphite oxide. Carbon 2007;45:1558–65.
[35] Park S, An J, Piner RD, Jung I, Yang D, Velamakanni A, et al. Aqueous suspension and characterization of chemically modified graphene sheets. Chem Mater 2008;20(21):6592–4.
[36] Ren PG, Yan DX, Ji X, Chen T, Li ZM. Temperature dependence of graphene oxide reduced by hydrazine hydrate. Nanotechnology 2011;22(5):055705.
[37] Kuila T, Bose S, Hong CE, Uddin ME, Khanra P, Kim NH, et al. Preparation of functionalized graphene/linear low density polyethylene composites by a solution mixing method. Carbon 2011;49(3):1033–7.
[38] Barzola-Quiquia J, Esquinazi P. Ferromagnetic- and superconducting-like behavior of the electrical resistance of an inhomogeneous graphite flake. J Supercond Novel Magn 2010;23(4):451–5.
[39] Bala Kumar S, Guo J. Modelling very large magnetoresistance of graphene nanoribbon devices. Nanoscale 2012;4:982–5.
[40] Bai J, Cheng R, Xiu F, Liao L, Wang M, Shailos A, et al. Very large magnetoresistance in graphene nanoribbons. Nat Nanotechnol 2010;5:655–9.
[41] Wang SW, Lin HE, Lin HD, Chen KY, Tu KH, Chen CW, et al. Transport behavior and negative magnetoresistance in chemically reduced graphene oxide nanofilms. Nanotechnology 2011;22:335701.
[42] Peres NMR, Neto AHC, Guinea F. Dirac fermion confinement in graphene. Phys Rev B 2006;73:241403.
[43] Peres NMR, Neto AHC, Guinea F. Conductance quantization in mesoscopic graphene. Phys Rev B 2006;73:195411.
[44] Huang YC, Chang CP, Lin MF. Magnetic and quantum confinement effects on electronic and optical properties of graphene ribbons. Nanotechnology 2007;18:495401.
[45] Liu J, Wright AR, Zhang C, Ma Z. Strong terahertz conductance of graphene nanoribbons under a magnetic field. Appl Phys Lett 2008;93:041106.
[46] Ritter C, Makler SS, Latgé A. Energy-gap modulations of graphene ribbons under external fields: a theoretical study. Phys Rev B 2008;77:195443.
[47] Li TS, Huang YC, Chang SC, Chang CP, Lin MF. Magnetoconductance of graphene nanoribbons. Philos Mag 2009;89(8):697–709.
[48] McCann E, Kechedzhi K, Fal'ko VI, Suzuura H, Ando T, Altshuler BL. Weak-localization magnetoresistance and valley symmetry in graphene. Phys Rev Lett 2006;97:146805.
[49] Gopinadhan K, Shin YJ, Yudhistira I, Niu J, Yang H. Giant magnetoresistance in single-layer graphene flakes with a gate-voltage-tunable weak antilocalization. Phys Rev B 2013;88:195429.